Dalton Transactions

ROYAL SOCIETY OF CHEMISTRY

PAPER

View Article Online
View Journal | View Issue

Cite this: *Dalton Trans.*, 2025, **54**, 16086

Unveiling the interplay: comparing solvent extraction, structure, and stability constants in a phenanthroline diamide system with trivalent lanthanides

Emma M. Archer, † Correy R. Vigil, † Shane S. Galley, Jessica A. Jackson and Jenifer C. Shafer *

Phenanthroline diamide ligands have shown promise as extractants for the selective separation of the An(III) from the Ln(III) in used nuclear fuel recycling. To enhance the effectiveness of these ligands, a fundamental understanding of their interactions with the full Ln(III) series is essential. In this study, the extraction behavior of the full Ln(III) series, including the typically unavailable Pm(III), was evaluated using the ligand *N*,*N*′,*N*,*N*′-tetraethylphenanthroline-2,9-diamide (TEtDAPhen). Solvent extraction experiments reveal a general trend of decreasing extraction efficiency from La(III) to Lu(III), which correlates inversely with the increasing thermodynamic stability constants of the corresponding Ln(TEtDAPhen)$(NO_3)_3$ complexes across the series. The stability constants suggest a lanthanide contraction effect, with stronger interactions with the increased charge density. Additionally, single-crystal X-ray diffraction analysis of the solid-state structures of Ln(III) complexes (excluding Pm(III)) provides valuable insight into the coordination environment and binding modes of the ligand. Together, these results help establish a structural relationship that informs the design and optimization of phenanthroline diamide ligands for An(III)/Ln(III) separations. The inclusion of Pm(III) in this study also offers a rare and comprehensive perspective across the entire lanthanide series.

Received 11th July 2025,
Accepted 24th September 2025

DOI: 10.1039/d5dt01636c

rsc.li/dalton

1. Introduction

Although nuclear energy continues to emerge as a compelling source of sustainable global energy, effective long-term nuclear waste management remains a challenge. One strategy to mitigate the radiotoxicity and heat load of used nuclear fuel is through selective separation of trivalent actinides (An(III)) from trivalent lanthanides (Ln(III)), which would enable transmutation of the more radiotoxic actinides and more efficient long-term storage of the remaining used nuclear fuel raffinate.[1,2] Achieving effective separation of the An(III) from the Ln(III) remains challenging due to the similar ionic radii and oxidation states of the An(III) and Ln(III).[3] The development of selective ligand systems that can exploit subtle differences in their electronic structures, such as nitrogen donor ligands and mixed nitrogen and oxygen (*N*,*O*-donor) ligands over oxygen donor ligands, must be explored further to support such strategies.[4–9]

N,*O*-donor ligands have demonstrated improved selectivity for the An(III) over the Ln(III) compared to purely oxygen-donating systems. Their favorable coordination chemistry, coupled with their ability to be fully incinerated reducing secondary waste, make *N*,*O*-donor ligands attractive candidates for use in solvent extraction processes.[10] A promising class of *N*,*O*-donor ligands, phenanthroline diamide (DAPhen) extractants, combine rigid aromatic frameworks of the phenanthroline backbone and tuneability of the amide arms.[11–13] While DAPhen-based extractants have shown promise in the separation of Am(III) from Eu(III), comprehensive studies across the full Ln(III) series remain limited. In particular, there is a lack of data involving Pm(III), which is often excluded as a result of its radioactivity and scarcity. This work addresses this gap by exploring the coordination behavior and extraction efficiency of the full Ln(III) series, including Pm(III), introducing new perspectives with TEtDAPhen, shown in Fig. 1.[14–17]

The work herein describes the characterization of the TEtDAPhen extractant in nitrate media with Ln(III) to analyze the relationship between the extraction selectivity, structural behavior, and binding strength of the Ln(III)-TEtDAPhen complexes. Selectivity is observed for the early Ln(III) compared to the late Ln(III) and shifts significantly between Eu(III) and Gd

Colorado School of Mines, 1500 Illinois St., Golden, Colorado, USA.
E-mail: jshafer@mines.edu
† These authors contributed equally to this work.

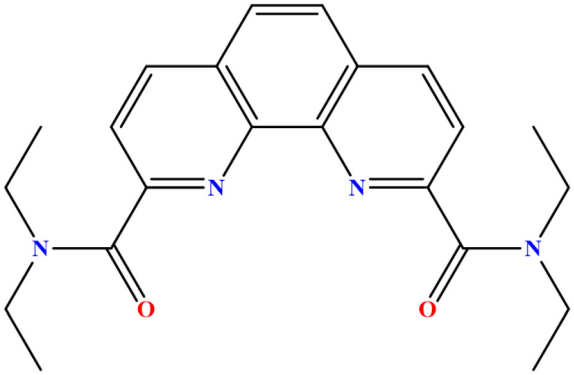

Fig. 1 Structure of the TEtDAPhen extractant.

(III). The extraction of Pm(III) is reported, representing a size analogue to Am(III), and follows the trend with the Ln(III) series. Distortion of the ligand in the crystal structure is observed across the Ln(III) series as the ligand attempts to accommodate the decreasing Ln(III) ionic radii. The stability constants across the Ln(III) series demonstrate a general trend of increasing with higher charge density, while reflecting the one-to-one metal-to-ligand speciation observed in the extraction and structural studies.

2. Experimental methods

2.1 Materials

Neocuproine hydrate (99%), selenium dioxide (ReagentPlus®, powder, 99.8% trace metals basis), 1,4-dioxane (ACS reagent, ≥99.0%), thionyl chloride (reagent grade, >97%), triethylamine (≥99.5%), diethylamine (≥99.5%), and nitrobenzene (ACS reagent, ≥99.0%) were purchased from Sigma-Aldrich and used as received. Nitric acid (ACS grade, 68–70%) used in this study was obtained from VWR and was diluted with 18 MΩ deionized water. Dichloromethane (Certified ACS), diethyl ether (anhydrous, ACS Grade), hexanes (Certified ACS), and acetonitrile (Optima® LC/MS) were purchased from Fisher Chemical.

2.2 Solvent extraction

The TEtDAPhen extractant was synthesized utilizing the method obtained from Zhang *et al.*[14] TEtDAPhen was verified to be >99% *via* GC-MS. TEtDAPhen was dissolved in nitrobenzene at concentrations of 0.05 M, 0.075 M, 0.1 M and 0.2 M. The organic phase was prepared by measuring the ligand in a volumetric flask and diluting to volume with nitrobenzene for each concentration at room temperature. A pre-equilibration step was performed with the organic phase by mixing with a 1 M HNO_3 aqueous phase that contained no metal using a volume ratio that matched the extraction step. The samples were prepared in accordance with the proper phase ratio utilized. The mixture was thoroughly mixed for 60 minutes at 2000 rpm using a Benchmark shaker table followed immediately by centrifugation at room temperature. The organic phase was isolated for solvent extraction with the lanthanide metals. The lanthanide metals were prepared in 1 M HNO_3 and all lanthanide concentrations were less than 10% of ligand concentration (or less than 0.5 mM). Phase ratios between 1 : 1–4 : 1 organic : aqueous were utilized to drive measurable extraction of the Ln(III). A 1 : 1 phase ratio was utilized for the extraction of ^{147}Pm. The aqueous phase was sampled (150 μL to 500 μL) using a micropipette and was then prepared for ICP-OES analysis by mass as the organic phase was unable to be directly measured. An initial aqueous sample was prepared to quantify the initial metal concentration of the aqueous phase. The samples were analyzed on a PerkinElmer Avio 200 ICP-OES. The distribution values (D) are used to evaluate the extraction performance of the experiment. The calculation is shown below in eqn (1).

$$D = \frac{A_i - A_f}{A_f} \times \text{PhaseRatio} \quad (1)$$

Caution! ^{147}Pm ($t_{1/2}$ = 2.6 years) and its daughters are serious health hazards due to the β emission of this radioisotope. This study was conducted in a laboratory equipped for radioactive studies and personnel wearing proper dosimetry. The ^{147}Pm solvent extraction measurements were performed at room temperature, with equal phase ratio, and in triplicate. The ^{147}Pm extraction solutions were prepared as described above. For the ^{147}Pm extraction, 13 000 dpm was added to each reaction vial to quantify the extraction and 100 μL samples were taken from the organic and aqueous phases and added to 6 mL of Ultima Gold AB scintillation cocktails. The samples were counted on a HIDEX 300 SL with data acquisition windows of 0–1023. The distribution value was obtained using eqn (2).

$$D = \frac{[M]_{org}}{[M]_{aq}} \times \text{PhaseRatio}. \quad (2)$$

2.3 Synthesis of *N*,*N*′,*N*,*N*′-tetraethyl-2,9-diamide-1,10-phenanthroline lanthanide(III) trinitrate; Ln(TEtDAPhen)$(NO_3)_3$

In a fume hood with no attempt to exclude air and moisture, a 100 mL beaker was charged with Ln_2O_3, where Ln = La(III), Ce (III), Sm(III), Eu(III), Gd(III), Dy(III), Ho(III), Er(III), Tm(III), Yb(III). The solid was dissolved in a minimum amount of $HNO_{3(aq)}$. The resulting translucent solutions were heated on a hot plate until the solution evaporated completely. Then, a minimum amount of 1 M $HNO_{3(aq)}$ was added to the solids, separately, to dissolve completely. These solutions were heated until the solution evaporated completely. Finally, a minimum amount of $H_2O_{(aq)}$ was added to the solids, separately, to dissolve completely. Heating was repeated until the solutions evaporated completely to obtain $Ln(NO_3)_3{\cdot}6H_2O$. 1-Dram vials were charged with the $Ln(NO_3)_3{\cdot}6H_2O$ and dissolved in 0.5 mL of CH_3CN. Meanwhile, separate 1-dram vials were charged with

TEtDAPhen and dissolved with CH_3CN to make a lightly brown solution. The TEtDAPhen solution was added slowly to the Ln $(NO_3)_3{\cdot}6H_2O$ containing flask. The 1-dram reaction flask was placed into a 20 mL scintillation vial that contained 3 mL of diethyl ether and was allowed to vapor diffuse overnight to form suitable crystals for X-ray diffraction. The mother liquor was removed by decantation and the complex was isolated by single crystal X-ray diffraction.

2.3.1 Synthesis of La(TEtDAPhen)$(NO_3)_3$. $La(NO_3)_3{\cdot}6H_2O$ was made using the procedure above. For the crystallization, 6.5 mg (0.015 mmol) of $La(NO_3)_3{\cdot}6H_2O$ and 13 mg (0.034 mmol) of TEtDAPhen was used (43% yield). NMR (500 MHz, Acetonitrile-D_3): δ 8.81 (d, 2H), 8.24 (d, 4H), 3.82 (q, 4H), 3.71 (q, 4H), 1.47 (t, 6H), 1.35 (t, 6H). IR: 1598 cm^{-1}, 1444 cm^{-1}, 1297 cm^{-1}, 1258 cm^{-1}, 1141 cm^{-1}, 716 cm^{-1}. Elemental analysis for $C_{22}H_{26}N_7O_{11}La$: calculated C, 48.45; H, 4.84; N, 14.24. Found C, 43.23; H, 4.35; N, 14.01.

2.3.2 Synthesis of Ce(TEtDAPhen)$(NO_3)_3$. $Ce(NO_3)_3{\cdot}6H_2O$ was made using the procedure above. For the crystallization, 5.2 mg (0.012 mmol) of $Ce(NO_3)_3{\cdot}6H_2O$ and 6.3 mg (0.019 mmol) of TEtDAPhen was used (43% yield). NMR (500 MHz, Acetonitrile-D_3): δ 10.08 (d, 2H), 9.53 (d, 2H), 8.08 (s, 2H), 7.54 (q, 4H), 5.19 (q, 4H), 3.39 (t, 6H), 2.51 (t, 6H). IR: 1599 cm^{-1}, 1444 cm^{-1}, 1273 cm^{-1}, 1258 cm^{-1}, 1099 cm^{-1}, 716 cm^{-1}. Elemental analysis for $C_{22}H_{26}N_7O_{11}Ce$: calculated C, 37.50; H, 3.72; N, 13.92. Found C, 37.54; H, 3.70; N, 13.95.

2.3.3 Synthesis of Sm(TEtDAPhen)$(NO_3)_3$. $Sm(NO_3)_3{\cdot}6H_2O$ was made using the procedure above. For the crystallization, 6.0 mg (0.013 mmol) of $Sm(NO_3)_3{\cdot}6H_2O$ and 5.9 mg (0.016 mmol) of TEtDAPhen was used (81% yield). NMR (500 MHz, Acetonitrile-D_3): δ 8.94 (d, 2H), 8.60 (d, 2H), 8.27 (s, 2H), 4.39 (q, 4H), 4.09 (q, 4H), 1.68 (m, 12H), 1.70. IR: 1596 cm^{-1}, 1469 cm^{-1}, 1286 cm^{-1}, 1030 cm^{-1}, 876 cm^{-1}, 735 cm^{-1}. Elemental analysis for $C_{22}H_{26}N_7O_{11}Sm$: calculated C, 36.96; H, 3.67; N, 13.72. Found C, 36.97; H, 3.63; N, 13.75.

2.3.4 Synthesis of Eu(TEtDAPhen)$(NO_3)_3$. $Eu(NO_3)_3{\cdot}6H_2O$ was made using the procedure above. For the crystallization, 6.3 mg (0.014 mmol) of $Eu(NO_3)_3{\cdot}6H_2O$ and 6.2 mg (0.016 mmol) of TEtDAPhen was used (73% yield). NMR is not reported due to paramagnetism. IR: 1596 cm^{-1}, 1459 cm^{-1}, 1278 cm^{-1}, 1031 cm^{-1}, 874 cm^{-1}, 712 cm^{-1}. Elemental analysis for $C_{22}H_{26}N_7O_{11}Eu$: calculated C, 36.88; H, 3.59; N, 13.61. Found C, 36.86; H, 3.59; N, 13.61.

2.3.5 Synthesis of Gd(TEtDAPhen)$(NO_3)_3$. $Gd(NO_3)_3{\cdot}6H_2O$ was made using the procedure above. For the crystallization, 6.2 mg (0.014 mmol) of $Gd(NO_3)_3{\cdot}6H_2O$ and 6.1 mg (0.016 mmol) of TEtDAPhen was used (75% yield). NMR is not reported due to paramagnetism. IR: 1598 cm^{-1}, 1469 cm^{-1}, 1289 cm^{-1}, 1031 cm^{-1}, 876 cm^{-1}, 713 cm^{-1}. Elemental analysis for $C_{22}H_{26}N_7O_{11}Gd$: calculated C, 36.61; H, 3.63; N, 13.59. Found C, 36.69; H, 3.56; N, 13.57.

2.3.6 Synthesis of Dy(TEtDAPhen)$(NO_3)_3$. $Dy(NO_3)_3{\cdot}6H_2O$ was made using the procedure above. For the crystallization, 6.2 mg (0.014 mmol) of $Dy(NO_3)_3{\cdot}6H_2O$ and 5.9 mg (0.016 mmol) of TEtDAPhen was used (71% yield). NMR is not reported due to paramagnetism. IR: 1599 cm^{-1}, 1469 cm^{-1}, 1294 cm^{-1}, 1033 cm^{-1}, 876 cm^{-1}, 713 cm^{-1}. Elemental analysis for $C_{22}H_{26}N_7O_{11}Dy$: calculated C, 36.35; H, 3.61; N, 13.49. Found C, 36.06; H, 3.46; N, 13.22.

2.3.7 Synthesis of Ho(TEtDAPhen)$(NO_3)_3$. $Ho(NO_3)_3{\cdot}6H_2O$ was made using the procedure above. For the crystallization, 7.5 mg (0.016 mmol) of $Ho(NO_3)_3{\cdot}6H_2O$ and 7.2 mg (0.019 mmol) of TEtDAPhen was used (70% yield). NMR is not reported due to paramagnetism. IR: 1599 cm^{-1}, 1468 cm^{-1}, 1288 cm^{-1}, 1033 cm^{-1}, 875 cm^{-1}, 712 cm^{-1}. Elemental analysis for $C_{22}H_{26}N_7O_{11}Ho$: calculated C, 36.23; H, 3.59; N, 13.44. Found C, 36.43; H, 3.52; N, 13.42.

2.3.8 Synthesis of Er(TEtDAPhen)$(NO_3)_3$. $Er(NO_3)_3{\cdot}6H_2O$ was made using the procedure above. For the crystallization, 7.1 mg (0.016 mmol) of $Er(NO_3)_3{\cdot}6H_2O$ and 7.0 mg (0.018 mmol) of TEtDAPhen was used (66% yield). NMR is not reported due to paramagnetism. IR: 1600 cm^{-1}, 1468 cm^{-1}, 1289 cm^{-1}, 1034 cm^{-1}, 875 cm^{-1}, 712 cm^{-1}. Elemental analysis for $C_{22}H_{26}N_7O_{11}Er$: calculated C, 36.11; H, 3.58; N, 13.40. Found C, 35.54; H, 3.45; N, 12.96.

2.3.9 Synthesis of Tm(TEtDAPhen)$(NO_3)_3$. $Tm(NO_3)_3{\cdot}6H_2O$ was made using the procedure above. For the crystallization, 8.0 mg (0.018 mmol) of $Tm(NO_3)_3{\cdot}6H_2O$ and 7.5 mg (0.020 mmol) of TEtDAPhen was used (54% yield). NMR is not reported due to paramagnetism. IR: 1600 cm^{-1}, 1466 cm^{-1}, 1289 cm^{-1}, 1034 cm^{-1}, 875 cm^{-1}, 712 cm^{-1}. Elemental analysis for $C_{22}H_{26}N_7O_{11}Tm$: calculated C, 36.03; H, 3.57; N, 13.37. Found C, 35.89; H, 3.47; N, 13.21.

2.3.10 Synthesis of Yb(TEtDAPhen)$(NO_3)_3$. $Yb(NO_3)_3{\cdot}6H_2O$ was made using the procedure above. For the crystallization, 6.2 mg (0.014 mmol) of $Yb(NO_3)_3{\cdot}6H_2O$ and 6.0 mg (0.016 mmol) of TEtDAPhen was used (46% yield). NMR (500 MHz, Acetonitrile-D_3): δ 2.26 (broad). IR: 1600 cm^{-1}, 1462 cm^{-1}, 1289 cm^{-1}, 1030 cm^{-1}, 879 cm^{-1}, 712 cm^{-1}. Elemental analysis for $C_{22}H_{26}N_7O_{11}Yb$: calculated C, 35.83; H, 3.55; N, 13.29. Found C, 35.44; H, 3.44; N, 12.93.

2.4 X-ray crystallography

Single crystals of Ln(TEtDAPhen)$(NO_3)_3$ (Ln: Ce, Sm, Eu, Gd, Dy, Ho, Er, Tm, Yb) suitable for X-ray diffraction were obtained as described in the synthetic procedures reported above. The Ln(TEtDAPhen)$(NO_3)_3$ crystals were individually submerged in mineral oil and mounted on a MiTeGen mount for data collection. The crystals were optically aligned on a Bruker D8 Venture X-ray diffractometer using a built-in camera. Preliminary measurements were performed using an I-μ-S X-ray source (Ag Kα, λ = 0.56086 Å) with high-brilliance and high-performance focusing quest multilayer optics. Data were collected, reflections were indexed and processed, and the files were scaled and corrected for absorption using APEX5. The reflection's intensities of a sphere were collected by a mixture of four sets of frames. Each set had a different omega angle for the crystal, and each exposure covered a range of 0.50 in ω, totaling 1464 frames. The frames were collected with an exposure time of 5. The space groups were assigned, and the structures were solved by direct methods using Olex2-1.5.

2.5 UV-Visible spectrophotometry

UV-Vis-NIR spectroscopy was carried out on a Varian Cary300 at room temperature. A 0.015 mM solution of TEtDAPhen was prepared by dissolving TEtDAPhen in acetonitrile. Meanwhile, 0.28 mM solutions of $La(NO_3)_3{\cdot}6H_2O$, $Pr(NO_3)_3{\cdot}6H_2O$, $Nd(NO_3)_3{\cdot}6H_2O$, $Sm(NO_3)_3{\cdot}6H_2O$, $Eu(NO_3)_3{\cdot}6H_2O$, and $Ho(NO_3)_3{\cdot}6H_2O$ were prepared in acetonitrile from the nitrate salts prepared previously. The 0.14 mM $Lu(NO_3)_3{\cdot}5H_2O$ solution was prepared from a 0.712 M $Lu(NO_3)_3{\cdot}5H_2O$ stock solution in acetonitrile. A 1-dram vial was initially charged with 2 mL of the 0.015 mM TEtDAPhen solution and subsequent 5 μL additions of $Ln(NO_3)_3{\cdot}XH_2O$ were added to the 1-dram vial and stirred for 1 minute to ensure homogeneity. For each scan, an 800 μL aliquot of the reaction vial was transferred to a quartz cuvette (1 cm pathlength) and this solution was assayed by UV-Vis spectroscopy. This process was repeated 30 or more times per metal solution, which transferred a total of 150 μL of each metal solution to the reaction vial in each titration case. Note, at the end of the titration a total of 2 $Ln(NO_3)_3{\cdot}XH_2O$ equivalents were added to 1 equivalent of TEtDAPhen. All UV-Vis measurements were made from 240–380 nm with a scan rate of 600 nm min^{-1} and interval of 1 nm. Data acquisition persisted until no change occurred in the spectral features. Stability constants and factor analysis were calculated and obtained in HypSpec2014 accounting for dilution of metal and ligand solutions.

3. Results and discussion

3.1 Solvent extraction

Trivalent lanthanide distribution with TEtDAPhen must be assessed to further evaluate the effective separation of An(III) from Ln(III) using DAPhen extractants and where the selectivity arises. These data can be used to compare and predict the behavior of other DAPhen extractants. The extraction experiments were completed using nitrobenzene as the organic diluent to facilitate comparison to the literature and to overcome the limited solubility of TEtDAPhen in aliphatic diluents. The extraction trend is reported in Fig. 2, which shows decreasing extraction across the Ln(III) series. This trend is consistent with what has been observed in the literature across the Ln(III) series.[18,19] Pm(III) distribution was characterized for this system and it was observed that for higher concentrations of TEtDAPhen, the Pm(III) distribution ratio was higher than that of Nd(III) and Sm(III) (the adjacent Ln(III)). The Pm(III) extraction trend followed the trend closer to its adjacent Ln(III) with lower concentrations of TEtDAPhen. The extraction of Pm(III) has previously been observed to be higher than that of the adjacent early Ln(III).[20] The increase in distribution value at Nd(III) and Pm(III) compared to La(III), Ce(III) and Pr(III) suggests that the ionic radii of Nd(III) and Pm(III) represent a good size match for the binding motif of TEtDAPhen. A steep decrease in the distribution ratio is consistently observed between Eu(III) and Gd(III) with varying [TEtDAPhen]. This relationship has previously been observed in the literature.[21] Low error distribution ratios were more difficult to obtain traversing across the Ln(III) as the distribution values decreased. At relatively low [TEtDAPhen], below 0.1 M TEtDAPhen, measurable distribution past Tb was not feasible, even with adjusted phase ratios, as a result of low extraction resulting in large error values.

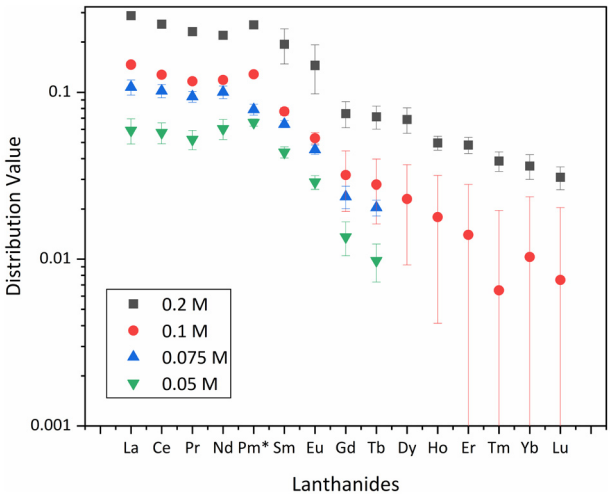

Fig. 2 Distribution values with respect to the Ln(III) series. Extractions performed at 1 M HNO_3 in the aqueous phase and nitrobenzene as the organic diluent.

Solvent extraction serves not only as a separation method but also as a tool for investigating M–L coordination chemistry. The efficiency and selectivity of extraction reflect the nature and strength of M–L interactions, offering an indirect yet powerful method for assessing complex formation across a series of metal ions. For this determination, ligand dependence experiments, where the aqueous phase conditions are held constant while varying the TEtDAPhen concentration in the organic phase, are conducted. From the ligand dependence solvent extraction experiments (Fig. S5–S14), slope analysis can be used to determine the M : L stoichiometry under these extraction conditions. The slope values range from 0.87 ± 0.06 to 1.21 ± 0.04 (1σ) indicating a one-to-one relationship between the Ln(III) and TEtDAPhen. This slope analysis in nitrobenzene is similar to that of a system using the tetrabutylated DAPhen (TBuDAPhen) in F-3 (3-nitrobenzotrifluoride), which showed slope numbers of 1.1 ± 0.1–1.5 ± 0.1.[22] These slope analysis results in F-3 or nitrobenzene have been observed in other systems, such as the tetradodecylated DAPhen (TDoDecDAPhen) and pyrrole and methylpyrrole substituted DAPhens (Pyr-DAPhen and MePyr-DAPhen).[23,24] This indicates that these systems form primarily one-to-one complexes in these polar and polar fluorinated diluents.

3.2 Crystallography

To explain the selectivity observed across the Ln(III) series by structural differences, a series of crystals were grown using vapor diffusion of diethyl ether into a reaction flask consisting

of acetonitrile. Suitable crystals for X-ray diffraction studies were grown within hours and evaluated by the ShelX suite software.[25,26] The crystallographic tables for: La(III), Ce(III), Sm (III), Eu(III), Gd(III), Dy(III), Ho(III), Er(III), Tm(III), and Yb(III) are shown in Tables S1–S10. The La(III) structure revealed an 11-coordinate geometry in which bonding occurs in a tetradentate fashion with one TEtDAPhen through the two nitrogen atoms on the phenanthroline, two oxygen atoms on the amide arms, an oxygen atom from a second TEtDAPhen, and in a bidentate fashion through six oxygen atoms from three nitrate anions, shown in Fig. 3. From Ce(III)–Tm(III), ten-coordinate structures were observed where bonding occurs in a tetradentate fashion with one TEtDAPhen through the two nitrogen atoms on the phenanthroline, two oxygen atoms on the amide arms, and in a bidentate fashion through six oxygen atoms from the three nitrate anions, Fig. 3. The Yb(TEtDAPhen)$(NO_3)_3$ structure resulted in a nine-coordinate geometry as a result of a monodentate coordination to a nitrate anion due to the smaller ionic size of Yb(III) compared to the other Ln(III) ions, Fig. 3. This was the same result observed for Lu(III) as seen previously.[27] These complexes reveal a one-to-one metal-to-ligand complex that is also observed in the solvent extraction slope analysis. The bond lengths are reported in Tables 1 and 2. The M–O_L, M–N, and M–O_{NO_3} are all comparable to the tetrabutyl-DAPhen (TBuDAPhen) system reported previously.[28,29]

Table 2 Reported bond lengths for the La(TEtDAPhen)$(NO_3)_3$ isomers. Bond lengths are reported in Å

Bond	Length (Å)	Bond	Length (Å)
La–O1	2.505(3)	La–O14	2.555(3)
La–O2	2.560(3)	La–O15	2.504(3)
La–O12	2.542(3)	La–O25	2.560(3)
La–N2	2.731(4)	La–N13	2.732(4)
La–N3	2.736(4)	La–N14	2.739(4)
La–$O3_{(NO_3)}$	2.651(3)	La–$O16_{(NO_3)}$	2.632(3)
La–$O4_{(NO_3)}$	2.638(3)	La–$O17_{(NO_3)}$	2.647(3)
La–$O6_{(NO_3)}$	2.611(3)	La–$O19_{(NO_3)}$	2.696(3)
La–$O7_{(NO_3)}$	2.699(3)	La–$O20_{(NO_3)}$	2.601(4)
La–$O9_{(NO_3)}$	2.700(4)	La–$O22_{(NO_3)}$	2.701(4)
La–$O10_{(NO_3)}$	2.761(4)	La–$O23_{(NO_3)}$	2.738(4)

There is noticeable asymmetry in the lengths of the M–O_L bonds from Ce(III)–Tm(III) where one bond is shorter than the other by ~0.06 Å with the exception of Pr(III), which has a difference of 0.01 Å. Similar asymmetry is observed in the M–N bond lengths from Ce(III)–Tm(III) with the exception of Pr(III) which has a difference of 0.002 Å. The small differences between the Pr(III)–O_L and Pr(III)–N bond lengths results in nearly symmetric bonding for the Pr(III) structure. The asymmetry in the M–O_L and M–N bond lengths describes the distortion that the ligand undergoes for complexation with the Ln(III).

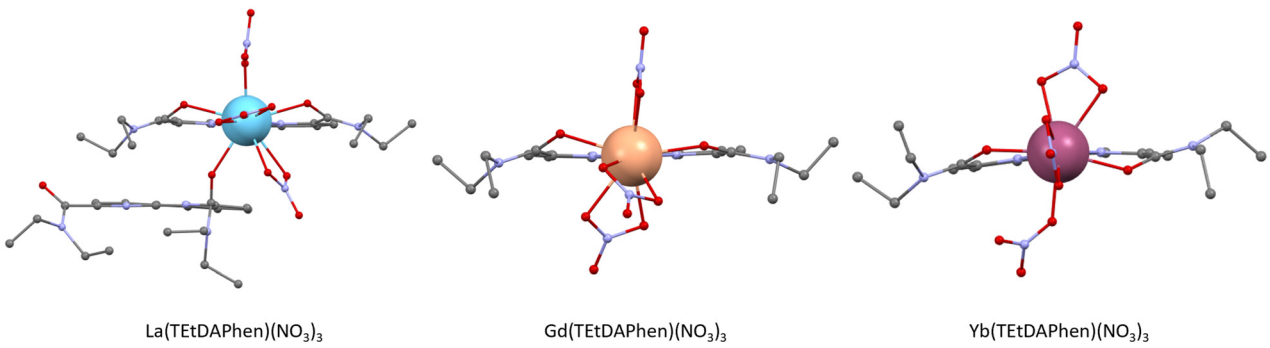

Fig. 3 Coordination modes of the M(TEtDAPhen)$(NO_3)_3$ system with M = La, Gd, and Yb representing the 11-, 10-, and 9-coordinate complexes and visualization of the distortion along the phenanthroline plane for the various coordination modes in the crystal structures.

Table 1 Reported bond lengths of the M(TEtDAPhen)$(NO_3)_3$ complexes where M = Ce, Sm, Eu, Gd, Dy, Ho, Er, Tm, Yb. Bond lengths are reported in Å

Bond	1-Ce	1-Sm	1-Eu	1-Gd	1-Dy	1-Ho	1-Er	1-Tm	1-Yb
M–O1	2.4421(12)	2.4521(16)	2.3777(13)	2.3782(15)	2.3493(14)	2.411(2)	2.342(3)	2.388(3)	2.289(2)
M–O2	2.5014(11)	2.3905(17)	2.4337(13)	2.4345(14)	2.4103(13)	2.353(2)	2.399(2)	2.334(3)	2.321(2)
M–N2	2.7107(12)	2.587(2)	2.6241(15)	2.6250(17)	2.5955(16)	2.531(3)	2.573(3)	2.509(3)	2.470(2)
M–N3	2.6542(13)	2.6444(19)	2.5656(15)	2.5657(17)	2.5366(16)	2.594(3)	2.519(3)	2.568(3)	2.442(2)
M–$O3_{(NO_3)}$	2.5809(12)	2.4870(16)	2.4615(13)	2.4894(16)	2.4603(15)	2.511(3)	2.448(3)	2.495(3)	2.482(2)
M–$O4_{(NO_3)}$	2.6259(12)	2.5105(17)	2.4853(14)	2.5408(16)	2.5205(15)	2.462(3)	2.498(3)	2.438(3)	2.385(2)
M–$O6_{(NO_3)}$	2.5783(12)	2.5003(17)	2.5207(14)	2.5218(15)	2.5004(15)	2.454(3)	2.492(3)	2.431(3)	2.368(2)
M–$O7_{(NO_3)}$	2.5702(12)	2.5307(18)	2.4780(14)	2.4765(15)	2.4502(14)	2.501(3)	2.438(3)	2.490(3)	2.394(2)
M–$O9_{(NO_3)}$	2.5729(12)	2.5104(18)	2.5374(14)	2.4884(15)	2.4649(14)	2.456(3)	2.449(3)	2.442(3)	2.258(9)
M–$O10_{(NO_3)}$	2.5602(11)	2.5644(18)	2.4859(15)	2.4636(14)	2.4337(14)	2.426(2)	2.403(2)	2.394(3)	—

The Yb(TEtDAPhen)$(NO_3)_3$ and Lu(TEtDAPhen)$(NO_3)_3$ M–O_L and M–N bond lengths show less asymmetry than the rest of the Ln(III) series which is an artifact of less steric hinderance of the nine-coordinate structure compared to the 10-coordiante structure of the rest of the Ce(III)–Tm(III). The M–O_L and M–N bond lengths in the Yb(III) and Lu(III) system differ only by ~0.03 Å which is less than that of the Ce(III)–Tm(III) structures. The distortion of the phenanthroline plane across the Ln(III) is shown in Fig. 4. This figure shows that both of the M–O_L bonds of the Ce(III)–(Tm) structures remain above the phenanthroline plane until Yb(III). The extent to which the M–O_L bonds extend above the phenanthroline plane vary slightly from Ce(III)–Tm(III). The distances of the M–OL bonds above the phenanthroline plane have consistent deviation in planarity across the Ln(III) series with the exception of the Pr(III) structure, published previously, where the two M–OL bonds had nearly symmetric distances from the phenanthroline backbone.[27] At Yb(III), the coordination shifts to 9-coordinate and the phenanthroline backbone bends to allow for one M–O_L bond to be above and the other below the phenanthroline plane. Similar observations have been made for the Lu(III) structure as well.[27] These results highlight the extreme extent that the DAPhen scaffold can distort to accommodate bonding to the smaller f-element ions. The late coordination shift from 10- to 9-coordinate marks an interesting place to observe a coordination number change in the Ln(III) series as this is often noticed earlier in the series. The distortion of the phenanthroline plane was observed earlier in the Ln(III) series in the TBuDAPhen system at Ho(III) where the M–OL bonds changed from being above the phenanthroline plane to above and below the phenanthroline plane.[28]

Furthermore, the bidentate coordination of the nitrate anions in the Ce(III)–Tm(III) systems with TEtDAPhen result in bicapped square antiprism geometries, shown in Fig. 3. The average Ln–$O_{(NO_3)}$ bond lengths are reflected in Tables 1 and 2. These ranges show a steady decrease in the bond lengths across the Ln(III) series from Ce(III)–Tm(III) with a steeper decrease at Yb(III). The M–nitrate bond lengths reported in this system are consistent with those of other systems prepared with $Ln(NO_3)_3$.[30]

To examine the significance of the bond length changes across the Ln(III) series, the average bond lengths were plotted against the nine-coordinate ionic radii from Shannon *et al.* in Fig. 5 and compared with the previously obtained Am(III) structure.[27,31] In this plot, it can be observed that the bond lengths decrease as ionic size decreases. However, there is a distinct shift in shorter bond lengths at Yb(III) and Lu(III) which is where the bidentate coordination of the three nitrate anions shifts to one monodentate nitrate anion and two bidentate nitrate anions. The shorter bond lengths at Yb(III) and Lu (III) are a reflection of decreasing steric bulk from the change of the bidentate to monodentate nitrate coordination. This represents a unique place in the Ln(III) series to observe this ionic radius induced shift in coordination. In the TBuDAPhen

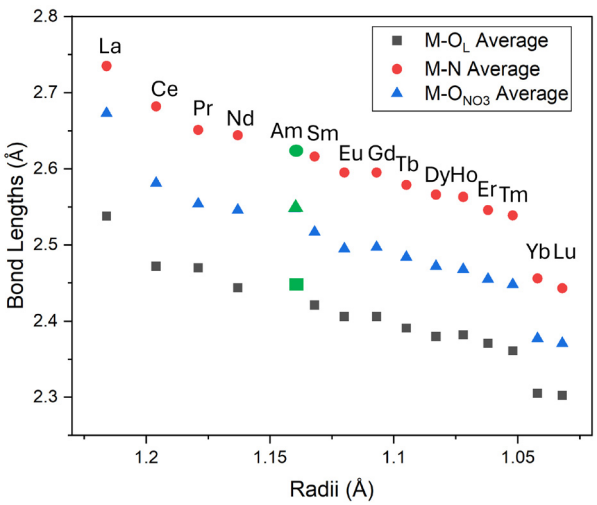

Fig. 5 Average bond lengths of the M–O_L, M–N, and M–$O_{(HNO_3)}$ bond lengths in the Ln(III) series with respect to the nine-coordinate ionic radii reported in Shannon *et al.*[31] The Pr(III), Nd(III), Tb(III), and Lu(III) structures are reported previously.[27]

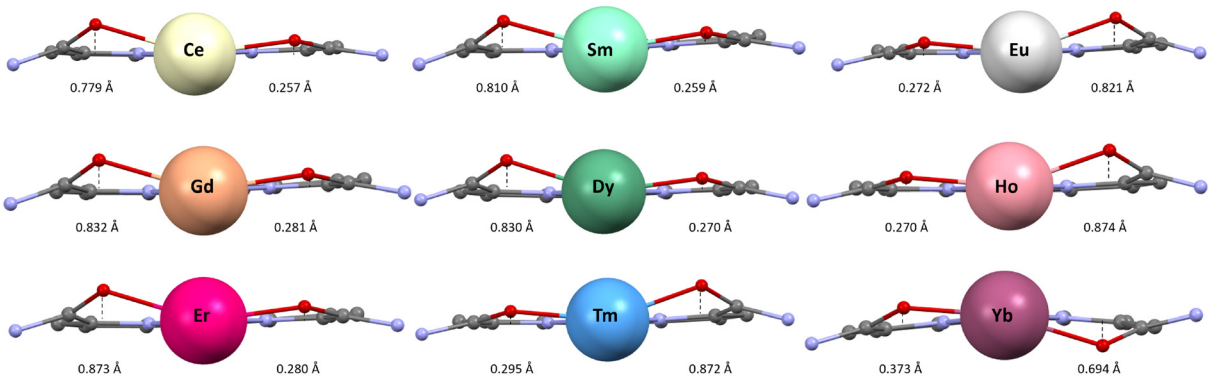

Fig. 4 Visualization of the distortion along the phenanthroline plane (with nitrate anions and ethyl groups omitted for clarity) for the reported Ln(III) crystal structures.

system, a coordination break from CN = 10 to CN = 9 happened at Ho(III) in the Ln(III) series which is a more common place for this to happen, although the TBuDAPhen is more bulky with the butyl chains on the amide arms.[28,29]

3.3 Stability constant determination

The speciation and complexation were further explored through UV-Visible spectrophotometric titrations in acetonitrile with titrations shown in Fig. 6. The stability constants of the Ln(III) complexes with TEtDAPhen were determined using HypSpec2014.[32,33] A wavelength range of 240–380 nm was isolated for analysis, which represents the ligand absorption band and is comparable to the literature.[17,24,34,35] Across the Ln(III) series, the stability constants increase from La(III) through Nd(III), decrease at Sm(III), then increase through Lu (III), Table 3. The observation of increasing stability constants across the Ln(III) series coupled with the decreasing extraction ability across the Ln(III) series has been observed in studies where both forms of analysis were completed.[24] The increasing stability constants have been attributed to the increasing charge density of the Ln(III) across the series and demonstrates the electrostatic interactions as the driving force of complexation. The decreasing distribution values across the series demonstrates the restriction of the size of the binding center.

Table 3 Measured stability constants in CH_3CN with TEtDAPhen reported at the 95% confidence level

Reaction	$\log \beta$
TEtDAPhen + $La(NO_3)_3 \rightleftharpoons La(TEtDAPhen)(NO_3)_3$	6.11 ± 0.05
TEtDAPhen + $Pr(NO_3)_3 \rightleftharpoons Pr(TEtDAPhen)(NO_3)_3$	6.17 ± 0.03
TEtDAPhen + $Nd(NO_3)_3 \rightleftharpoons Nd(TEtDAPhen)(NO_3)_3$	6.48 ± 0.03
TEtDAPhen + $Sm(NO_3)_3 \rightleftharpoons Sm(TEtDAPhen)(NO_3)_3$	5.99 ± 0.04
TEtDAPhen + $Ho(NO_3)_3 \rightleftharpoons Ho(TEtDAPhen)(NO_3)_3$	6.25 ± 0.05
TEtDAPhen + $Lu(NO_3)_3 \rightleftharpoons Lu(TEtDAPhen)(NO_3)_3$	6.55 ± 0.06

Throughout the analysis of the spectrophotometric titration data, a one-to-one M : L complex was determined to be the primary species using principal component analysis. The 1 : 1 $\log \beta_1$ values obtained for this system in CH_3CN are higher than the pyrrolidinated DAPhen (Pyr-DAPhen) for La(III) by ~0.14 log units, ~0.47 log units for Nd(III), and ~0.48 log units for Lu(III).[24] The trend remains the same between the TEtDAPhen and Pyr-DAPhen systems and within the same order of magnitude.[17] The Sm(III) stability constant from this work is within the same order of magnitude as the stability constant obtained for the TEtDAPhen system providing good comparison.

Comparing the stability constant, crystallographic, and extraction results, the data would suggest there may be an opti-

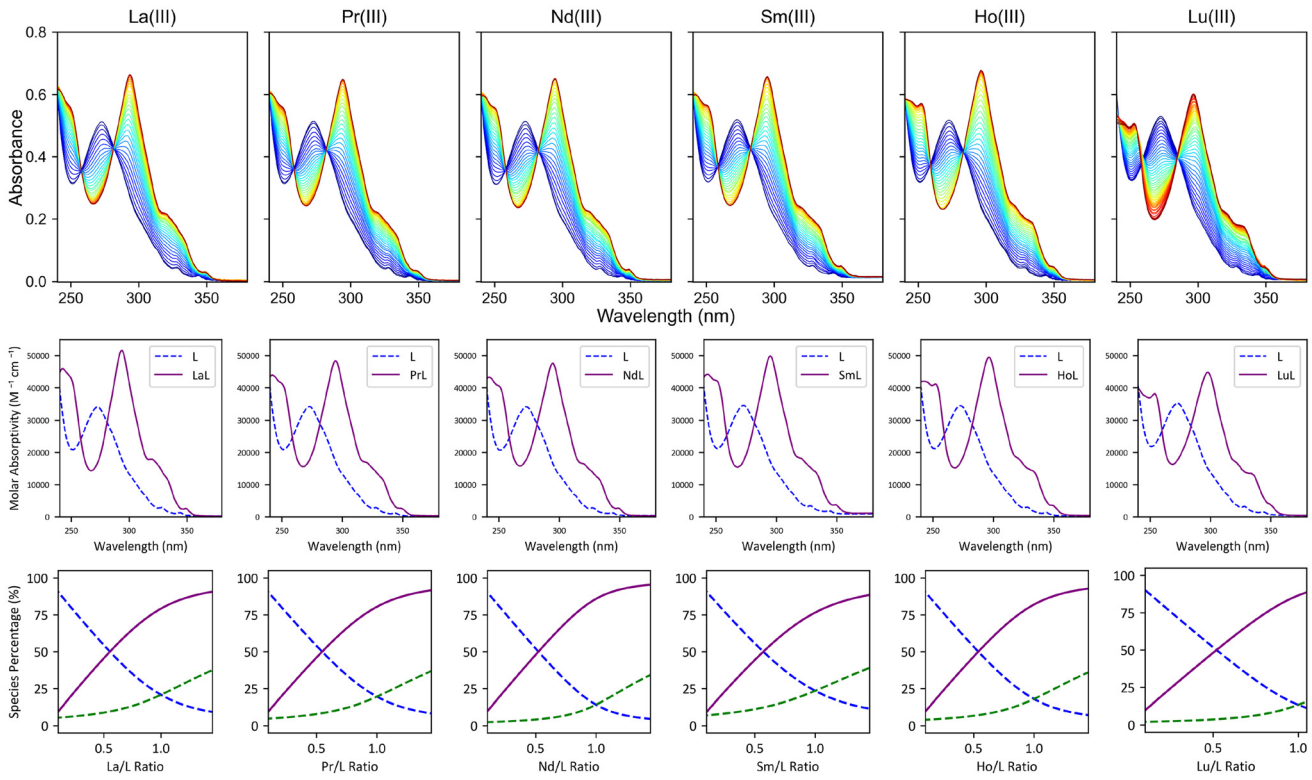

Fig. 6 (Top) UV-Visible spectrophotometric titrations of $La(NO_3)_3$, $Pr(NO_3)_3$, $Nd(NO_3)_3$, $Sm(NO_3)_3$, $Ho(NO_3)_3$, and $Lu(NO_3)_3$ in CH_3CN. [TEtDAPhen] = 0.015 mM, $[La(NO_3)_3]$ = 0.28 mM, $[Pr(NO_3)_3]$ = 0.28 mM, $[Nd(NO_3)_3]$ = 0.28 mM, $[Sm(NO_3)_3]$ = 0.28 mM, $[Ho(NO_3)_3]$ = 0.28 mM, $[Lu(NO_3)_3]$ = 0.14 mM, V_i = 2 mL of TEtDAPhen solution with 5 μL additions of $La(NO_3)_3$, $Pr(NO_3)_3$, $Nd(NO_3)_3$, $Sm(NO_3)_3$, $Ho(NO_3)_3$, and $Lu(NO_3)_3$, respectively. (Middle) Molar absorptivity of the free TEtDAPhen and $M(TEtDAPhen)(NO_3)_3$ complex. (Bottom) Speciation diagram of the formation of the $M(TEtDAPhen)(NO_3)_3$ complexes with free metal (green dash), free ligand (blue dash), and complex (purple) plotted.

mized size match between Pr(III) and Pm(III) which can be observed in the extraction data by the higher distribution value of Pm(III) comparatively, in the stability constant determination with Nd(III) having a larger stability constant than the adjacent Ln(III), and in the symmetry observed in the Pr(III) crystal structure. Similar findings have been observed in the 2,9-di(pyrid-2-yl)-1,10-phenanthroline system which found increased thermodynamic stability at Sm(III) indicating strong size selectivity for that range of ionic size.[36]

4. Conclusions

The characterization and quantification of bonding interactions of the TEtDAPhen ligand with the whole Ln(III) series has highlighted interesting behavior across the series. Through the comprehensive analysis of this system using solvent extraction, X-ray crystallography, and spectrophotometric titrations, the interactions between the Ln(III) and TEtDAPhen have shown insights into DAPhen complexation and separation affinity and the interplay of the different bonding interactions contributing to the system. This work has shown the extraction behavior of Pm(III) with TEtDAPhen in the context of the full Ln(III) series. The decreasing affinity observed in solvent extraction studies across the Ln(III) series could allow for size-based targeting of different An(III) or Ln (III) in creative separations designs. Observing the Ln(III) structures with TEtDAPhen through crystallographic means has provided insight into the bonding distortion of the DAPhen moiety which is complementary to the systems in which crystal structures cannot be obtained. The comparison of the distribution values of the Ln(III) in a biphasic extraction system with the stability constants determined in a monophasic system, the size and electronically driven interactions, respectively, can be isolated. These characterization methods can inform further ligand design for targeting the lighter or heavier lanthanides for rare earth element separations, or for optimization of the separation of An(III) from the Ln(III).

Author contributions

EMA: conceptualization, methodology, investigation, data curation, formal analysis, visualization, writing – original draft, writing – review and editing. CRV: data curation, validation, writing – review and editing. JAJ: visualization, writing – review and editing. SSG: formal analysis, writing – review and editing. JCS: funding acquisition, project administration, writing – review and editing.

Conflicts of interest

There are no conflicts to declare.

Data availability

The data supporting this article have been included as part of the supplementary information (SI). Supplementary information is available. See DOI: https://doi.org/10.1039/d5dt01636c.

CCDC 2450883 (La), 2450881 (Ce), 2450523 (Sm), 2450882 (Eu), 2450524 (Gd), 2450520 (Dy), 2450519 (Ho), 2450521 (Er), 2450522 (Tm), and 2450518 (Yb) contain the supplementary crystallographic data for this paper.[37a–j]

Acknowledgements

We would like to thank the U.S. Department of Energy Office of Science, Office of Basic Energy Sciences, and Colorado School of Mines for supporting this work under award number DE-SC0020189 (E. M. A., C.R.V., S. S. G., J. A. J., and J. C. S.).

References

1 L. R. Morss, N. M. Edelstein and J. Fuger, *The Chemistry of the Actinide and Transactinide Elements Third Edition*, 2008, pp. 2622–2768.
2 K. L. Nash and J. C. Braley, *Nuclear Energy and the Environment*, 2010, pp. 19–38.
3 K. L. Nash, *Solvent Extr. Ion Exch.*, 1993, **11**, 729–768.
4 P. J. Panak and A. Geist, *Chem. Rev.*, 2013, **113**, 1199–1236.
5 F. W. Lewis, L. M. Harwood, M. J. Hudson, M. G. Drew, A. Wilden, M. Sypula, G. Modolo, T.-H. Vu, J.-P. Simonin, G. Vidick, N. Bouslimani and J. F. Desreux, *Procedia Chem.*, 2012, **7**, 231–238.
6 F. W. Lewis, L. M. Harwood, M. J. Hudson, M. G. Drew, V. Hubscher-Bruder, V. Videva, F. Arnaud-Neu, K. Stamberg and S. Vyas, *Inorg. Chem.*, 2013, **52**, 4993–5005.
7 A. Bhattacharyya and P. K. Mohapatra, *Radiochim. Acta*, 2019, **107**, 931–949.
8 A. Leoncini, J. Huskens and W. Verboom, *Chem. Soc. Rev.*, 2017, **46**, 7229–7273.
9 A. A. Peroutka, S. S. Galley and J. C. Shafer, *Coord. Chem. Rev.*, 2023, **482**, 1–31.
10 S. W. Long, *The Incineration of Low-Level Radioactive Waste A Report for the Advisory Committee on Nuclear Waste U.S. Nuclear Regulatory Commission Advisory Committee on Nuclear Waste*, U.s. nuclear regulatory commission technical report, 1990.
11 E. M. Archer, S. S. Galley, J. A. Jackson and J. C. Shafer, *Solvent Extr. Ion Exch.*, 2023, **41**, 697–740.
12 X. Yang, L. Xu, D. Fang, A. Zhang and C. Xiao, *Chem. Commun.*, 2024, **60**, 11373–11598.
13 L. Xu, X. Yang, A. Zhang, C. Xu and C. Xiao, *Coord. Chem. Rev.*, 2023, **496**, 215404.
14 X. Zhang, L. Yuan, Z. Chai and W. Shi, *Sci. China: Chem.*, 2018, **61**, 1285–1292.

15 Y. Li, X. Yang, P. Ren, T. Sun, W. Shi, J. Wang, J. Chen and C. Xu, *Inorg. Chem.*, 2021, **60**, 5131–5139.
16 X. Zhang, X. Kong, L. Yuan, Z. Chai and W. Shi, *Inorg. Chem.*, 2019, **58**, 10239–10247.
17 S. Wang, X. Yang, Y. Liu, L. Xu, C. Xu and C. Xiao, *Inorg. Chem.*, 2024, **63**, 3063–3074.
18 X. F. Yang, P. Ren, Q. Yang, J. S. Geng, J. Y. Zhang, L. Y. Yuan, H. B. Tang, Z. F. Chai and W. Q. Shi, *Inorg. Chem.*, 2021, **60**, 9745–9756.
19 M. Simonnet, T. Kobayashi, K. Shimojo, K. Yokoyama and T. Yaita, *Inorg. Chem.*, 2021, **60**(17), 13409–13418.
20 X. Zhang, Q. Wu, J. Lan, L. Yuan, C. Xu, Z. Chai and W. Shi, *Sep. Purif. Technol.*, 2019, **223**, 274–281.
21 M. V. Evsiunina, P. I. Matveev, P. Kalle, E. K. Khult, P. S. Lemport, N. A. Avagyan, V. G. Petrov, Y. A. Ustynyuk and V. G. Nenajdenko, *Inorg. Chem.*, 2025, **64**, 3311–3325.
22 M. Alyapyshev, J. Ashina, D. Dar'In, E. Kenf, D. Kirsanov, L. Tkachenko, A. Legin, G. Starova and V. Babain, *RSC Adv.*, 2016, **6**, 68642–68652.
23 N. Tsutsui, Y. Ban, H. Suzuki, M. Nakase, S. Ito, Y. Inaba, T. Matsumura and K. Takeshita, *Anal. Sci.*, 2020, **36**, 241–246.
24 P. S. Lemport, M. V. Evsiunina, P. I. Matveev, V. S. Petrov, A. S. Pozdeev, E. K. Khult, Y. V. Nelyubina, K. L. Isakovskaya, V. A. Roznyatovsky, I. P. Gloriozov, B. N. Tarasevich, A. S. Aldoshin, V. G. Petrov, S. N. Kalmykov, Y. A. Ustynyuk and V. G. Nenajdenko, *Inorg. Chem. Front.*, 2022, **9**, 4402–4412.
25 G. M. Sheldrick, *Acta Crystallogr., Sect. C:Struct. Chem.*, 2015, **71**, 3–8.
26 O. V. Dolomanov, L. J. Bourhis, R. J. Gildea, J. A. K. Howard and H. Puschmann, *J. Appl. Crystallogr.*, 2009, **42**, 339–341.
27 E. M. Archer, F. A. Pereiro, J. M. Riley, E. B. Flynn, J. C. Gilhula, B. L. Huffman, J. A. Jackson, J. G. Knapp, B. N. Long, H. E. Mason, M. S. Mullis, S. A. Kozimor, J. C. Shafer and S. S. Galley, *Inorg. Chem. Front.*, 2025, DOI: 10.1039/d5qi01056j.
28 A. V. Yatsenko, M. V. Evsiunina, Y. V. Nelyubina, K. L. Isakovskaya, P. S. Lemport, P. I. Matveev, V. G. Petrov, V. A. Tafeenko, A. S. Aldoshin, Y. A. Ustynyuk and V. G. Nenajdenko, *Polyhedron*, 2023, **243**, 2–15.
29 P. S. Lemport, M. V. Evsiunina, Y. V. Nelyubina, K. L. Isakovskaya, V. N. Khrustalev, V. S. Petrov, A. S. Pozdeev, P. I. Matveev, Y. A. Ustynyuk and V. G. Nenajdenko, *Mendeleev Commun.*, 2021, **31**, 853–855.
30 B. Ahrens, S. A. Cotton, N. Feeder, O. E. Noy, P. R. Raithby and S. J. Teat, *J. Chem. Soc., Dalton Trans.*, 2002, 2027–2030.
31 R. D. Shannon, *Acta Crystallogr.*, 1976, **32**, 751–767.
32 P. Gans, A. Sabatini and A. Vacca, *Talanta*, 1996, **43**, 1739–1753.
33 P. Gans, A. Sabatini and A. Vacca, *Ann. Chim.*, 1999, **89**, 45–49.
34 R. Meng, L. Xu, X. Yang, M. Sun, C. Xu, N. E. Borisova, X. Zhang, L. Lei and C. Xiao, *Inorg. Chem.*, 2021, **60**, 8754–8764.
35 C. L. Xiao, C. Z. Wang, L. Y. Yuan, B. Li, H. He, S. Wang, Y. L. Zhao, Z. F. Chai and W. Q. Shi, *Inorg. Chem.*, 2014, **53**, 1712–1720.
36 A. N. Carolan, G. M. Cockrell, N. J. Williams, G. Zhang, D. G. Vanderveer, H. S. Lee, R. P. Thummel and R. D. Hancock, *Inorg. Chem.*, 2012, **52**, 15–27.
37 (*a*) CCDC 2450883: Experimental Crystal Structure Determination, 2025, DOI: 10.5517/ccdc.csd.cc2n8br1; (*b*) CCDC 2450881: Experimental Crystal Structure Determination, 2025, DOI: 10.5517/ccdc.csd.cc2n8bpz; (*c*) CCDC 2450523: Experimental Crystal Structure Determination, 2025, DOI: 10.5517/ccdc.csd.cc2n7z41; (*d*) CCDC 2450882: Experimental Crystal Structure Determination, 2025, DOI: 10.5517/ccdc.csd.cc2n8bq0; (*e*) CCDC 2450524: Experimental Crystal Structure Determination, 2025, DOI: 10.5517/ccdc.csd.cc2n7z52; (*f*) CCDC 2450520: Experimental Crystal Structure Determination, 2025, DOI: 10.5517/ccdc.csd.cc2n7z1y; (*g*) CCDC 2450519: Experimental Crystal Structure Determination, 2025, DOI: 10.5517/ccdc.csd.cc2n7z0x; (*h*) CCDC 2450521: Experimental Crystal Structure Determination, 2025, DOI: 10.5517/ccdc.csd.cc2n7z2z; (*i*) CCDC 2450522: Experimental Crystal Structure Determination, 2025, DOI: 10.5517/ccdc.csd.cc2n7z30; (*j*) CCDC 2450518: Experimental Crystal Structure Determination, 2025, DOI: 10.5517/ccdc.csd.cc2n7yzv.